

Influence of biomass burning from South Asia at a high-altitude mountain receptor site in China

Jing Zheng¹, Min Hu^{1,*}, Zhuofei Du¹, Dongjie Shang¹, Zhaoheng Gong^{2,a}, Yanhong Qin¹, Jingyao Fang¹, Fangting Gu¹, Mengren Li¹, Jianfei Peng¹, Jie Li³, Yuqia Zhang³, Xiaofeng Huang², Lingyan He², Yusheng Wu¹, Song Guo¹

¹State Key Joint Laboratory of Environmental Simulation and Pollution Control, College of Environmental Sciences and Engineering, Peking University, Beijing, China

²Key Laboratory for Urban Habitat Environmental Science and Technology, School of Environment and Energy, Peking University Shenzhen Graduate School, Shenzhen, China

³State Key Laboratory of Atmospheric Boundary Layer Physics and Atmospheric Chemistry (LAPC), Nansen-Zhu International Research Center (NZC), Institute of Atmospheric Physics, Chinese Academy of Sciences, Beijing, China

* *Correspondence to:* minhu@pku.edu.cn

^a Now at John A. Paulson School of Engineering and Applied Sciences, Harvard University, Cambridge, Massachusetts, 02138, United States

Abstract

Highly time-resolved in-situ measurements of airborne particles were made at Mt. Yulong (3410 m above sea level) on the southeastern edge of the Tibetan Plateau in China from 22nd March to 14th April in 2015. Detailed chemical composition was measured by a high-resolution time-of-flight aerosol mass spectrometer together with other online instruments. Average mass concentration of the submicron particles (PM₁) was $5.7 \pm 5.4 \mu\text{g m}^{-3}$ during the field campaign, ranging from $0.1 \mu\text{g m}^{-3}$ up to $33.3 \mu\text{g m}^{-3}$. Organic aerosol (OA) was the dominant component in PM₁, with a fraction of 68%. Three OA factors, i.e., biomass-burning organic aerosol (BBOA), biomass-burning-influenced oxygenated organic aerosol (OOA-BB) and oxygenated organic aerosol (OOA), were resolved using positive matrix factorization analysis. The two oxygenated OA factors accounted for 87% of the total OA mass. Three biomass burning events were identified by examining the enhancement of black carbon concentrations and the f_{60} (the ratio of the signal at m/z 60 from the mass spectrum to the total signal of OA).

25 Back trajectories of air masses and satellite fire map data were integrated to identify the biomass burning locations and
26 pollutants transport. The western air masses from South Asia with active biomass burning activities transported large amount
27 of air pollutants, resulting in elevated organic concentrations up to 4-fold higher than that of the background condition. This
28 study at Mt. Yulong characterizes the tropospheric background aerosols of the Tibetan Plateau during pre-monsoon season,
29 and provides clear evidence that the southeastern edge of the Tibetan Plateau is affected by transport of anthropogenic aerosols
30 from South Asia.

31 **1 Introduction**

32 Aerosols play an important role in the radiative balance in earth's atmosphere, with their radiative forcing still having large
33 uncertainties (IPCC, 2013). Biomass burning emission is one of the dominant sources of atmospheric particles (von
34 Schneidemesser et al., 2015), contributing up to 90% of the primary organic aerosol in the global scale (Bond et al., 2004) and
35 more than half of the total organic aerosol mass in areas with significant biomass burning influences (e.g. Yangtze River Delta
36 region in China, and Indian Peninsula) (Zhang et al., 2015;Engling and Gelencser, 2010). Given the long atmospheric lifetime
37 of aerosols, even remote areas can sometimes be influenced by the transportation of air pollutants from areas with active
38 biomass burnings (Bougiatioti et al., 2014). In terms of the deterioration of air quality and climate change in those remote
39 areas, great scientific interest has arisen focusing on the impacts on biomass burning (Lau et al., 2010;Qian et al., 2011).

40 The Tibetan Plateau is the largest and highest plateau in the world, and is often regarded as the "Third Pole". It is surrounded
41 by a ring of high-elevated mountain ranges, which were considered as blocks for transportations of air pollutants from its
42 vicinity (Wang and French, 1994). Since this vast land has a relatively low population density with minor anthropogenic
43 influences, the Tibetan Plateau has been considered as a natural background of the Eurasian continent (Ming et al., 2010;Wan
44 et al., 2015). In recent years, studies have presented convincing evidence for the transport route of air pollutants climbing over
45 the Himalayas, especially during pre-monsoon season, coinciding with the annual intensive fire season in South and Southeast
46 Asia (Streets et al., 2003;Marinoni et al., 2010;Cong et al., 2015b). A westerly dry circulation helps to build up the smoke

47 plume against the Himalayan ridges, elevating to 3-5 km in altitude (Bonasoni et al., 2010;Xia et al., 2011). Subsequently,
48 downward glacier wind of local mountain breeze circulation brings biomass burning related air pollutants down to the mountain
49 valley (Cong et al., 2015b;L üthi et al., 2015).

50 A host of studies based on field campaigns have amassed an impressive amount of information describing the biomass
51 burning influence on different areas of the Tibetan Plateau (Decesari et al., 2010;Zhao et al., 2013;Xu et al., 2015). Those
52 studies were mostly approached by analyzing the temporal and spatial variations of atmospheric composition based on filter
53 measurements. The strong correlation of carbonaceous aerosol with biomass burning tracers K^+ and levoglucosan pointed out
54 the origins of aerosols (Cong et al., 2015a). Biomass burning organic aerosol (BBOA) was also found to be a major fraction
55 of organic aerosol (OA), with a 15% contribution to the total OA mass (Du et al., 2015). Xu et al. (2013) and You et al. (2016)
56 also presented convincing evidence about biomass burning impacts by analyzing chemical components in glaciers collected in
57 the Tibetan Plateau. Most of previous studies were based on offline analysis using filter or glacier samples, which were limited
58 to low time resolution, making it difficult to follow the aging process of biomass burning aerosol. Thus in-situ measurements
59 of aerosol chemical characterization with high time resolution are needed, so as to have a deep understanding of the sources
60 and evolution of the particulate matter.

61 In this study, the influence of biomass burning from South Asia on the Tibetan Plateau has been analyzed. The results can
62 serve as inputs or constraints for global climate model simulations. By examining the aerosol properties as a function of
63 chemical composition at Mt. Yulong at the southeastern edge of the Tibetan Plateau, this study sheds light on the evolution
64 processes of OA. Positive matrix factorization analysis has been conducted to resolve different sources of OA. And the
65 influence of biomass burning from South Asia transported over long distances to the Tibetan Plateau background environment
66 during pre-monsoon season has been characterized.

67 **2 Method**

68 **2.1 Site description and meteorological conditions during the campaign**

69 In this study, we conducted an intensive observation at the site on Mt. Yulong (27.2 N, 100.2 E), with an altitude of 3410 m
70 a.s.l., northwestern Yunnan Province, China (Fig.1). Since Mt. Yulong is lying in the transition zone extending from the low
71 altitudes of the Yunnan Plateau (~ 3000 a.s.l.) to the high altitude of the Tibetan Plateau (~ 5000 a.s.l.), it is on the transport
72 route of pollutants from South Asia to inland China, making it an ideal site to observe the influence of regional and long-range
73 transport of polluted air masses. This station is a member of the National Atmospheric Watch Network coordinated by the
74 Chinese Environmental Monitoring Center. The famous tourist attraction Lijiang Old Town locates more than 20 km away and
75 1000 m lower than the elevation of the station. The observation period was conducted during the pre-monsoon season of the
76 Tibetan Plateau, from 22nd March to 14th April 2015, corresponding to the annual biomass burning seasons in South Asia.
77 Since the season was cold with sparse visitors in Lijiang old city, the influence of local emissions from residents and visitors
78 remained low compared with other seasons.

79 **2.2 Measurements and data processing**

80 A high resolution time-of-flight aerosol mass spectrometer (AMS hereafter) was deployed to measure the highly time-
81 resolved chemical composition of sub-micron, non-refractory aerosols (Table S1). The standard operation procedures of the
82 AMS has been described in detail in Canagaratna et al. (2007). The time resolution was 5 min for AMS measurement, with
83 2.5 min in V mode to obtain mass concentration, and 2.5 min in W mode for HR mass spectrum of organics. The detection
84 limits (DL) of organic, sulfate, nitrate, ammonium and chloride were 0.07, 0.004, 0.003, 0.005 and 0.01 $\mu\text{g m}^{-3}$, respectively.
85 During most time of the campaign, the mass concentrations of chloride were below its DL, and including it would lower the
86 total signal to noise ratio, therefore it is omitted from the analysis.

87 The AMS data was analyzed using the standard AMS data analysis software, i.e., SQUIRREL (version 1.57) for unit
88 resolution mass spectrum data, and PIKA (version 1.16) for high resolution mass spectra data. Calibrations of the AMS on

89 flow rate and ionization efficiency were conducted each week. To account for the particle loss due to the bounce of particles
90 on the vaporizer, collection efficiencies were calculated and applied for data correction based on the method described by
91 Middlebrook et al. (2012). In this study, the collection efficiencies varied from 0.5 to 0.9.

92 The high resolution organic aerosol spectra were further apportioned to different sources by positive matrix factorization
93 (PMF) analysis (Paatero and Tapper, 1994;Ulbrich et al., 2009). The solution was validated by the characteristics of resolved
94 mass spectra, as well as the comparison of temporal variations between each factor and external species (e.g. acetonitrile).

95 Other online instruments were also deployed at the site (Table S1). A scanning mobility particle sizer (SMPS) was used to
96 measure particle number size distribution for particle mobility diameters ranging from 15 to 760 nm, with a time resolution of
97 5 min. An Aethalometer was deployed to measure the aerosol light absorption coefficients σ_{ap} at its seven wavelengths, ranging
98 from 370 to 950 nm. Black carbon (BC) concentration is determined by σ_{ap} at 880 nm using the default mass attenuation cross
99 sections of $16.6 \text{ m}^2 \text{ g}^{-1}$ (Fröhlich et al., 2015). Acetonitrile was measured by a gas chromatographer with mass spectrometer
100 and flame ionization detectors (GC–MS/FID) with a time resolution of 1 hour. Technical details of this self-made instrument
101 were described elsewhere (Wang et al., 2016).

102 Meteorological parameters, including relative humidity, temperature, wind direction and wind speed, were continuously
103 monitored on the site during the campaign. The low temperature ($5 \text{ }^\circ\text{C}$ for the whole campaign average) and heavy snow
104 eliminated the influence of biogenic emissions to this site during the campaign.

105 **2.3 Back trajectory analysis and fire maps**

106 To explore the influence of regional biomass burning activities on aerosol properties during the campaign, the Weather
107 Research and Forecasting (WRF) model (version 3.61) was used to investigate the meteorological conditions and to compute
108 trajectories of air masses arriving at Mt. Yulong. 48-h back trajectories were calculated every 6 hours from March 22nd to
109 April 14th, using a starting height at 600 m above the ground level of the site.

110 Active fire points were obtained from the Fire Information for Resource Management System (FIRMS), which is provided

111 by the Moderate Resolution Imaging Spectroradiometer (MODIS) satellite (<https://firms.modaps.eosdis.nasa.gov/firemap/>,
112 last accessed on Aug. 26, 2016).

113 **3 Results**

114 **3.1 Concentrations and chemical compositions of submicron aerosols**

115 The time series of submicron aerosol compositions as well as meteorological conditions are shown in Fig.2. The average
116 PM_{10} concentration was $5.7 \pm 5.4 \mu\text{g m}^{-3}$, with a range of $0.1 \mu\text{g m}^{-3} - 33.3 \mu\text{g m}^{-3}$. This result was similar to previous
117 observations at the Northern Tibetan Plateau, where Du et al. (2015) reported an average PM_{10} concentration of $11.4 \mu\text{g m}^{-3}$ in
118 the autumn of 2013, and Xu et al. (2014a) reported an annual average $PM_{2.5}$ concentration of $9.5 \mu\text{g m}^{-3}$ from 2006 to 2007.
119 The averaged PM_{10} concentration was much lower than those measured at urban and downwind sites of China (e.g., Huang et
120 al., 2013; Xu et al., 2014b), but was three times higher than the $1.7 \mu\text{g m}^{-3}$ at a background site in Europe in March 2004
121 (Sjogren et al., 2008), and ten times higher than that measured at the same background site in the spring of 2013 (Fröhlich et
122 al., 2015). These huge differences indicate that anthropogenic pollutions in South Asia may have resulted in the elevation of
123 aerosol concentrations to levels above the natural background level.

124 Averaged aerosol composition of PM_{10} is shown in the pie chart (Fig.3(a)). The PM_{10} chemical composition was dominated
125 by organic components, which accounted for 68%, followed by sulfate (14%). The minor contribution of nitrate to PM_{10} (4%)
126 can be explained by the lack of nearby anthropogenic sources for precursors (e.g., HONO, N_2O_5) (Du et al., 2015). This result
127 presents a similar picture as those observed at remote sites in the northern hemisphere (Zhang et al., 2011), as well as at a high
128 altitude site in Europe (Ripoll et al., 2015). Compared with urban or regional areas in China, where secondary inorganic species
129 including sulfate, nitrate and ammonium typically contribute to over one half of the total mass concentrations, the result at this
130 site is quite unique (Huang et al., 2010; Huang et al., 2012; Xu et al., 2014b).

131 Fig. 3(b) shows the relative contribution of major chemical components as a function of PM_{10} mass concentrations, as well
132 as the probability density of PM_{10} mass loading. PM_{10} concentrations below $5 \mu\text{g m}^{-3}$ showed the highest probability (68%). The

133 fractions of organics and BC increase slightly with the increasing of PM₁ concentrations, showing that they were the main
134 contributors to the pollution episodes in Mt. Yulong.

135 The PM₁ components did not show distinct diel variations, but remained relatively constant during the whole day, as shown
136 in Fig.3(c). This is similar to the findings at the Puy-de-Dôme station in central France, and the Montsec station in western
137 Mediterranean Basin (Freney et al., 2011; Ripoll et al., 2015). Strong long-range transport of air masses with few local
138 emissions could blur the diel cycles, since the air-mass transportations occurred regardless of the local time of the day.

139 **3.2 Characterization of organic aerosol**

140 **3.2.1 Elemental compositions of organic aerosol**

141 The elemental composition was calculated from high resolution mass spectra of organics obtained by AMS, using the
142 method developed by Canagaratna et al. (2015). Compared with the previous method (Aiken et al., 2007;2008), the ratio of
143 O/C and H/C are typically increased by 20% and 7%, respectively. Bulk OA was mainly composed of carbon and oxygen, with
144 minor contributions from hydrogen and nitrogen, and had an average molecular formula of C₁H_{1.4}O_{1.1}N_{0.04}. The fragments of
145 organics were grouped into five types according to the existence of C, H, O or N atoms. C_xH_y⁺ were only 21% of the total
146 organic signal, while the oxygenated fraction (C_xH_yO_z⁺) accounted for 68% of the total OA, which is higher than those
147 measured at urban and downwind site (30-41%) (Huang et al., 2011; Sun et al., 2011; Hu et al., 2013). The average OM/OC
148 and O/C ratios for the whole campaign were 2.63 and 1.11, respectively, and were similar to those measured in the north
149 eastern region of the Tibetan Plateau (OM/OC 2.75, O/C 1.16) (Xu et al., 2015). These results are slightly higher than the
150 elemental ratios measured at another remote site (OM/OC: 2.4, O/C: 0.9) in the eastern Mediterranean (Bougiatioti et al., 2014),
151 probably due to the mixture of free troposphere aerosol after a long time of processing before arriving at this high altitude site.
152 The extremely high value of OM/OC reflects the highly oxidized nature of OA in the Tibetan Plateau.

153 **3.2.2 Source apportionment of organic aerosol**

154 PMF analysis was performed to investigate the sources of OA measured at Mt. Yulong. Three factors were resolved,

155 including a biomass burning organic aerosol (BBOA), an oxygenated biomass-burning-influenced organic aerosol (OOA-BB),
156 and an oxygenated organic aerosol (OOA). Details of the PMF analysis can be found in the supplement. The mass spectra of
157 the three factors are shown in Fig. 4. The time series of the three factors and an external species (acetonitrile) are plotted in
158 Fig. 5.

159 3.2.2.1 BBOA

160 BBOA has been frequently identified in previous studies at urban and regional sites (Zhang et al., 2011). The mass spectrum
161 of BBOA has a notable contribution from m/z 60 (mainly $C_2H_4O_2^+$, contributing 3.1% of the total mass spectra), which is from
162 fragmentation of levoglucosan. As shown in Table 1, the mass spectrum correlates well with the samples from an aircraft
163 measurement above a large forest fire (Brito et al., 2014), and well with the samples from biomass burning simulation system
164 in the laboratory (He et al., 2010). BBOA has an O/C ratio of 0.37, presenting a similar level to previous studies (Aiken et al.,
165 2008;He et al., 2010). The time series of BBOA correlates very well with K^+ based on filter analysis (Pearson $R=0.92$, $N=13$).
166 The factor was also confirmed to be BBOA, since it has a similar temporal variation to that of acetonitrile (Fig.5), a gas phase
167 tracer for biomass burning.

168 The average concentration of BBOA was $0.5 \mu g m^{-3}$ for the whole campaign, accounting for 13% of the total OA mass, with
169 a maximum contribution at 61% (Fig.6 (a)). The spikes in the time series of BBOA indicate that a fraction of BBOA was
170 contributed by primary sources nearby, possibly occasional biomass burning activities for domestic heating and cooking. The
171 increasing fraction of BBOA as a function of total OA concentrations points to contributions from biomass burning activities
172 during the pollution episodes (Fig.6 (b)).

173 3.2.2.2 OOA-BB

174 The mass spectrum of OOA-BB factor was dominated by $C_xH_yO_z^+$ fragments, especially org29 (CHO^+), org43 ($C_2H_3O^+$)
175 and org44 (CO_2^+). The spectrum of OOA-BB in this study well correlated with aged BBOA obtained 3 hours downwind of a
176 forest fire (Brito et al., 2014) (Pearson $R=0.97$, $N=100$). It is qualitatively similar to published OOA-BB spectra from aged
177 BB plumes in China during the harvest seasons (Zhang et al., 2015), and also presented many similarities to those of OOA2-

178 BBOA resolved in the metropolitan area of Paris (Crippa et al., 2013).

179 The average concentration of OOA-BB was $0.9 \mu\text{g m}^{-3}$ for the whole campaign, accounting for 22% of the total OA mass.
180 Compared with BBOA measured near sources, OOA-BB shows a higher oxygenated degree, with an O/C of 0.85, and a
181 lower fraction of m/z 60 (0.6%), as a result of the oxidation of primary levoglucosan-type species (Jolleys et al., 2015). This
182 oxidation process can be quick in elevating the oxidation state and reducing f_{60} (calculated as the ratio of the signal at m/z 60
183 to the total OA signal), which is also reported in another study by Minguillón et al. (2015). As the plumes originated from
184 South Asia were measured at a distance of several hundred kilometers downwind, emissions would have undergone
185 substantial aging prior to sampling. The aging process includes both the gas-phase oxidation of semi volatile species from
186 biomass burning sources and heterogeneous or homogeneous reactions of existing particles during long-range transport
187 (Bougiatioti et al., 2014). The time series of OOA-BB and BBOA yield modest correlations with BC (Pearson R=0.62 and
188 0.65, N=5940). If we focus on the total biomass burning related organic aerosols (OOA-BB + BBOA), the R value for its
189 correlation with BC would increase to 0.76 (N=5940), indicating biomass burning related OA originated from the same
190 source as BC.

191 3.2.2.3 OOA

192 OOA is described as highly oxidized, aged particles formed after long-range transportation and processing. The mass
193 spectral properties of OOA are defined by having a dominant peak at m/z 44 (mainly CO_2^+) and other ions of $\text{C}_x\text{H}_y\text{O}_z^+$. The
194 highly oxidized nature of OOA is also reflected by its high O/C ratio of 1.45. The mass spectrum of OOA resembles that of
195 more oxidized OOA (MO-OOA) in Beijing well (Pearson R=0.69, N=100) (Hu et al., 2016).

196 OOA has an average concentration of $2.6 \mu\text{g m}^{-3}$, accounting for 65% of the total OA mass. Unlike previous studies at urban
197 or regional sites (Jimenez et al., 2009; Li et al., 2015; Hu et al., 2016), the time series of OOA did not agree well with that of
198 sulfate (Pearson R=0.32, N=5940), which was also the case at the puy-de-Dome research station (1465 m a.s.l.) (Freney et al.,
199 2011). The low Pearson correlation value can be partially explained by the extremely high concentration of OOA formed from
200 the oxidation of organics emitted by biomass burning activities during the first week of the campaign. For the rest of campaign,

201 the correlation value for sulfate with respect to OOA factor increased to 0.77 (N=5940), which is consistent with previous
202 studies.

203 As shown in Fig. 6(a), the two OOA factors (OOA-BB and OOA) were very abundant, with a predominantly contribution
204 of 87% to the total OA mass. This is consistent with the high oxygen level in the total OA. During 80% of the observation
205 period, OA concentrations were lower than $5 \mu\text{g m}^{-3}$, with strong contributions from secondary organic aerosols (OOA and
206 OOA-BB) (Fig.6 (b)). This indicates that the background site was predominated by organic aerosols formed through regional
207 transportation.

208 **4 Discussion**

209 **4.1 Identification of biomass burning events**

210 Enhanced BC concentrations were used to help identifying periods influenced by biomass burning plumes (Bougiatioti et
211 al., 2014). The BC concentration of 85 ng m^{-3} was taken as the background concentration at this site. It is the average
212 concentration observed in the beginning of April (1st April to 4th April), when the strong wind scavenged pollutants of the
213 whole region. Back trajectory and fire maps illustrate that the dominant air masses for this period was from north India with
214 minor biomass burning activities (see Fig.7(d)). This concentration is consistent with the two-year averaged background level
215 measured at Southern Himalayas (Marinoni et al., 2010), and comparable to the lowest BC concentrations found over the
216 southeastern Tibetan Plateau in the pre-monsoon season (Engling et al., 2011).

217 During the sampling period, three episodes were identified as being influenced by biomass burning, with the following
218 criteria satisfied, i.e. (a) Back trajectory analysis shows a uniform source region; (b) Fire map shows fire spots in the region
219 during the episode; (c) BC concentrations were higher than the background level of 85 ng m^{-3} determined above. One long-
220 lasting and strong episode was from 22nd March to 30th March. The air masses arrived at the site during this period were from
221 the north part of Myanmar, and covered active biomass burning areas (see Fig.7(a)). As shown on the fire map, the site may
222 also be influenced by wildfires in the vicinity. Two less intense events were observed on 5th – 6th April and 11th – 12th April,

223 with slightly elevated BC concentrations. During the third event (11th – 12th April), the site experienced heavy snow. The
224 back trajectory shows that air masses to this region were transported from regions with few fire spots. The enhanced BC
225 concentration was probably emitted by biomass burning activities nearby for domestic heating and cooking.

226 These three biomass burning events were further validated by the increase of the fraction of biomass burning tracers, f_{60} .
227 During the first and second events, the average f_{60} were 0.98% and 0.61%, respectively. These values were much lower than
228 the f_{60} of 1.4% during the third event, which was influenced by fires in the vicinity. This showed the decay of f_{60} in ambient
229 plumes transported from sources to the receptor site. During the clean episode, the f_{60} decreased to about 0.4%, indicating
230 minor biomass burning influence (Cubison et al., 2011).

231 The box plot (Fig.8) shows the concentrations of different chemical components of biomass burning events and background
232 conditions. The aerosol concentrations corresponding to the background condition is highlighted by light gray. Organic
233 aerosols are represented by the left axis while other species are represented by the right axis. Aerosols corresponding to biomass
234 burning events were at high concentrations. The concentrations of organic aerosol during three biomass burning events were
235 10, 4 and 6-fold higher than that of the background condition. During the first event, due to co-occurrence of biomass burning
236 activities in the vicinity together with the long-range transport of biomass burning plume, the concentration of BC reached 14
237 times higher than that of the background condition. All species remained low and sustained background concentrations during
238 the clean episode, with an average PM_1 concentration of $1.2 \mu g m^{-3}$.

239 **4.2 Characteristic of three Biomass burning events**

240 The comparison of OA fractions of different biomass burning events is shown in Fig.9. Since the air masses arriving at Mt.
241 Yulong during the second event were transported from active biomass burning areas in Myanmar within 48h, most of the
242 freshly emitted BBOA were processed and transformed to more oxidized OA, with OOA and OOA-BB together accounting
243 for 90% on average of the total organic mass. Although the ratio of BBOA to the total OA during this event has a similar level
244 to the background level, the mass concentrations of both OA and BBOA were more elevated than the background level. In

245 contrast, the fraction of BBOA had strong enhancement during the third event, reaching 23%. It is consistent with the
246 previously mentioned identification that the biomass burning plumes were mainly from residential heating nearby, which could
247 emit large amount of fresh BBOA.

248 The aging and/or mixing processes of different biomass burning plumes are further characterized in terms of the f_{44} vs. f_{60}
249 triangle plot (Cubison et al., 2011). f_{44} , similarly defined to f_{60} as the ratio of the signal at m/z 44 to the total OA signal, is used
250 here as an indicator of atmospheric aging, since OA and their gas phase precursors evolve in the atmosphere by becoming
251 increasingly oxidized with higher CO_2^+ fraction (Jimenez et al., 2009; Ng et al., 2010). BBOA can be clearly distinguished
252 from oxidized OA in the triangle plot. With the aging process of biomass burning plumes, OA evolved toward higher f_{44} and
253 lower f_{60} , and gained more similar signature with OOA.

254 The OA clusters of three biomass burning events are shown clearly in the f_{44} - f_{60} triangle plot (Fig.10). The OA clusters of
255 the first and third events both present OA peaks with high f_{60} values, since the site was possibly influenced by residential
256 heating in the surrounding regions during these two episodes. The OA cluster of the second event presents more similar
257 oxidative properties to OOA and OOA-BB, due to loss of biomass burning marker through aging process during transport.

258 **5 Conclusions**

259 During the pre-monsoon season the aerosol evolution was explored at a high altitude receptor site on Mt. Yulong (3410 m
260 a.s.l.) in the Tibetan Plateau in Southwestern China. The average concentration of PM_{10} was $5.7 \mu\text{g m}^{-3}$, which was far below
261 that measured in urban and suburban as well as regional sites of China. The carbonaceous species (OA+BC) were very
262 abundant in PM_{10} , with an average contribution of 77%, followed by sulfate (14%) and ammonium (5%). This high altitude
263 mountain site is suitable for tracing the influence of pollution plumes transported from the large areas of South Asia.

264 Using PMF analysis, organic aerosol was resolved into three factors, BBOA, OOA-BB and OOA. OOA-BB formed after
265 atmospheric process of BBOA during long-range transport. The two oxygenated OA factors (OOA and OOA-BB) accounted
266 for 87% of the total OA, showing the highly oxidized nature of aerosol at the Mt. Yulong.

267 Different types of biomass burning events were identified by examining organic tracer in mass profiles and BC
268 concentrations. The origins of biomass burning plumes were verified by analyzing the back trajectories of air masses as well
269 as fire maps. Elevated PM₁ concentrations due to the transport of air pollutants from active biomass burning areas in South
270 Asia were observed. Domestic heating activity also had interference on the background condition of Mt. Yulong.

271 This study provides clear evidence on the influence of the transport of pollutants emitted by biomass burning activity in
272 South Asia on the southeastern edge of the Tibetan Plateau in China. The chemical characteristics of aerosols observed by in
273 situ measurement can serve as inputs for model validations of aerosol-cloud processes and long-range transports. This study
274 also highlights the impact of anthropogenic emissions to the pristine region of the Tibetan Plateau, which may influence global
275 climate.

276

277 **Acknowledgements**

278 This study was supported by the National Natural Science Foundation of China (91544214, 21190052 and 41121004) and
279 the China Ministry of Environmental Protection's Special Funds for Scientific Research on Public Welfare (20130916). We
280 also thank China National Environmental Monitoring Center for the support to the field campaign.

281

282 **References**

- 283 Aiken, A. C., DeCarlo, P. F., and Jimenez, J. L.: Elemental Analysis of Organic Species with Electron Ionization High-
284 Resolution Mass Spectrometry, *Anal. Chem.*, 79, 8350-8358, 10.1021/ac071150w, 2007.
- 285 Aiken, A. C., Decarlo, P. F., Kroll, J. H., Worsnop, D. R., Huffman, J. A., Docherty, K. S., Ulbrich, I. M., Mohr, C., Kimmel,
286 J. R., Sueper, D., Sun, Y., Zhang, Q., Trimborn, A., Northway, M., Ziemann, P. J., Canagaratna, M. R., Onasch, T. B., Alfarra,
287 M. R., Prevot, A. S. H., Dommen, J., Duplissy, J., Metzger, A., Baltensperger, U., and Jimenez, J. L.: O/C and OM/OC Ratios
288 of Primary, Secondary, and Ambient Organic Aerosols with High-Resolution Time-of-Flight Aerosol Mass Spectrometry,
289 *Environ. Sci. Technol.*, 42, 10.1021/es703009q, 2008.
- 290 Bonasoni, P., Laj, P., Marinoni, A., Sprenger, M., Angelini, F., Arduini, J., Bonafè U., Calzolari, F., Colombo, T., Decesari, S.,
291 Di Biagio, C., di Sarra, A. G., Evangelisti, F., Duchi, R., Facchini, M. C., Fuzzi, S., Gobbi, G. P., Maione, M., Panday, A.,
292 Roccatò, F., Sellegri, K., Venzac, H., Verza, G. P., Villani, P., Vuillermoz, E., and Cristofanelli, P.: Atmospheric Brown Clouds

293 in the Himalayas: first two years of continuous observations at the Nepal Climate Observatory-Pyramid (5079 m), *Atmos.*
294 *Chem. Phys.*, 10, 7515-7531, 10.5194/acp-10-7515-2010, 2010.

295 Bougiatioti, A., Stavroulas, I., Kostenidou, E., Zampas, P., Theodosi, C., Kouvarakis, G., Canonaco, F., Prévôt, A. S. H.,
296 Nenes, A., Pandis, S. N., and Mihalopoulos, N.: Processing of biomass-burning aerosol in the eastern Mediterranean during
297 summertime, *Atmos. Chem. Phys.*, 14, 4793-4807, 10.5194/acp-14-4793-2014, 2014.

298 Brito, J., Rizzo, L. V., Morgan, W. T., Coe, H., Johnson, B., Haywood, J., Longo, K., Freitas, S., Andreae, M. O., and Artaxo,
299 P.: Ground-based aerosol characterization during the South American Biomass Burning Analysis (SAMBBA) field experiment,
300 *Atmos. Chem. Phys.*, 14, 12069-12083, 10.5194/acp-14-12069-2014, 2014.

301 Canagaratna, M. R., Jayne, J. T., Jimenez, J. L., Allan, J. D., Alfarra, M. R., Zhang, Q., Onasch, T. B., Drewnick, F., Coe, H.,
302 Middlebrook, A., Delia, A., Williams, L. R., Trimborn, A. M., Northway, M. J., DeCarlo, P. F., Kolb, C. E., Davidovits, P., and
303 Worsnop, D. R.: Chemical and microphysical characterization of ambient aerosols with the aerodyne aerosol mass spectrometer,
304 *Mass Spectrom. Rev.*, 26, 185-222, 10.1002/mas.20115, 2007.

305 Canagaratna, M. R., Jimenez, J. L., Kroll, J. H., Chen, Q., Kessler, S. H., Massoli, P., Ruiz, L. H., Fortner, E., R. Williams, L.,
306 R. Wilson, K., Surratt, J. D., Donahue, N. M., Jayne, J. T., and R. Worsnop, D.: Elemental ratio measurements of organic
307 compounds using aerosol mass spectrometry: characterization, improved calibration, and implications, *Atmospheric*
308 *Chemistry and Physics*, 15, 253–272, 10.5194/acp-15-253-2015, 2015.

309 Cong, Z., Kang, S., Kawamura, K., Liu, B., Wan, X., Wang, Z., Gao, S., and Fu, P.: Carbonaceous aerosols on the south edge
310 of the Tibetan Plateau: concentrations, seasonality and sources, *Atmos. Chem. Phys.*, 15, 1573-1584, 10.5194/acp-15-1573-
311 2015, 2015a.

312 Cong, Z., Kawamura, K., Kang, S., and Fu, P.: Penetration of biomass-burning emissions from South Asia through the
313 Himalayas: new insights from atmospheric organic acids, *Sci. Rep.*, 5, 9580, 10.1038/srep09580, 2015b.

314 Crippa, M., DeCarlo, P. F., Slowik, J. G., Mohr, C., Heringa, M. F., Chirico, R., Poulain, L., Freutel, F., Sciare, J., Cozic, J., Di
315 Marco, C. F., Elsasser, M., Nicolas, J. B., Marchand, N., Abidi, E., Wiedensohler, A., Drewnick, F., Schneider, J., Borrmann,
316 S., Nemitz, E., Zimmermann, R., Jaffrezo, J. L., Prevot, A. S. H., and Baltensperger, U.: Wintertime aerosol chemical
317 composition and source apportionment of the organic fraction in the metropolitan area of Paris, *Atmospheric Chemistry and*
318 *Physics*, 13, 961-981, 10.5194/acp-13-961-2013, 2013.

319 Cubison, M. J., Ortega, A. M., Hayes, P. L., Farmer, D. K., Day, D., Lechner, M. J., Brune, W. H., Apel, E., Diskin, G. S.,
320 Fisher, J. A., Fuelberg, H. E., Hecobian, A., Knapp, D. J., Mikoviny, T., Riemer, D., Sachse, G. W., Sessions, W., Weber, R. J.,
321 Weinheimer, A. J., Wisthaler, A., and Jimenez, J. L.: Effects of aging on organic aerosol from open biomass burning smoke in
322 aircraft and laboratory studies, *Atmospheric Chemistry and Physics*, 11, 12049-12064, 10.5194/acp-11-12049-2011, 2011.

323 Decesari, S., Facchini, M. C., Carbone, C., Giulianelli, L., Rinaldi, M., Finessi, E., Fuzzi, S., Marinoni, A., Cristofanelli, P.,
324 Duchi, R., Bonasoni, P., Vuillermoz, E., Cozic, J., Jaffrezo, J. L., and Laj, P.: Chemical composition of PM₁₀ and PM₁ at the
325 high-altitude Himalayan station Nepal Climate Observatory-Pyramid (NCO-P) (5079 m a.s.l.), *Atmos. Chem. Phys.*, 10, 4583-
326 4596, 10.5194/acp-10-4583-2010, 2010.

327 Du, W., Sun, Y. L., Xu, Y. S., Jiang, Q., Wang, Q. Q., Yang, W., Wang, F., Bai, Z. P., Zhao, X. D., and Yang, Y. C.: Chemical

328 characterization of submicron aerosol and particle growth events at a national background site (3295 m a.s.l.) on the Tibetan
329 Plateau, *Atmospheric Chemistry and Physics*, 15, 10811-10824, 10.5194/acp-15-10811-2015, 2015.

330 Engling, G., and Gelencser, A.: Atmospheric Brown Clouds: From Local Air Pollution to Climate Change, *Elements*, 6, 223-
331 228, 10.2113/gselements.6.4.223, 2010.

332 Engling, G., Zhang, Y.-N., Chan, C.-Y., Sang, X.-F., Lin, M., Ho, K.-F., Li, Y.-S., Lin, C.-Y., and Lee, J. J.: Characterization
333 and sources of aerosol particles over the southeastern Tibetan Plateau during the Southeast Asia biomass-burning season,
334 *Tellus B*, 63, 117-128, 10.1111/j.1600-0889.2010.00512.x, 2011.

335 Fröhlich, R., Cubison, M. J., Slowik, J. G., Bukowiecki, N., Canonaco, F., Croteau, P. L., Gysel, M., Henne, S., Herrmann, E.,
336 Jayne, J. T., Steinbacher, M., Worsnop, D. R., Baltensperger, U., and Prévôt, A. S. H.: Fourteen months of on-line
337 measurements of the non-refractory submicron aerosol at the Jungfraujoch (3580 m a.s.l.) – chemical composition, origins and
338 organic aerosol sources, *Atmospheric Chemistry and Physics*, 15, 11373-11398, 10.5194/acp-15-11373-2015, 2015.

339 Freney, E. J., Sellegri, K., Canonaco, F., Boulon, J., Hervo, M., Weigel, R., Pichon, J. M., Colomb, A., Prévôt, A. S. H., and
340 Laj, P.: Seasonal variations in aerosol particle composition at the puy-de-Dôme research station in France, *Atmos. Chem. Phys.*,
341 11, 13047-13059, 10.5194/acp-11-13047-2011, 2011.

342 He, L. Y., Lin, Y., Huang, X. F., Guo, S., Xue, L., Su, Q., Hu, M., Luan, S. J., and Zhang, Y. H.: Characterization of high-
343 resolution aerosol mass spectra of primary organic aerosol emissions from Chinese cooking and biomass burning, *Atmospheric
344 Chemistry and Physics*, 10, 11535-11543, 10.5194/acp-10-11535-2010, 2010.

345 Hu, W. W., Hu, M., Yuan, B., Jimenez, J. L., Tang, Q., Peng, J. F., Hu, W., Shao, M., Wang, M., Zeng, L. M., Wu, Y. S., Gong,
346 Z. H., Huang, X. F., and He, L. Y.: Insights on organic aerosol aging and the influence of coal combustion at a regional receptor
347 site of central eastern China, *Atmospheric Chemistry and Physics*, 13, 10095-10112, 10.5194/acp-13-10095-2013, 2013.

348 Hu, W. W., Hu, M., Hu, W., Jimenez, J. L., Yuan, B., Chen, W. T., Wang, M., Wu, Y. S., Chen, C., Wang, Z. B., Peng, J. F.,
349 Zeng, L. M., and Shao, M.: Chemical composition, sources, and aging process of submicron aerosols in Beijing: Contrast
350 between summer and winter, *JGRD*, 121, 1955-1977, 10.1002/2015jd024020, 2016.

351 Huang, X.-F., Xue, L., Tian, X.-D., Shao, W.-W., Sun, T.-L., Gong, Z.-H., Ju, W.-W., Jiang, B., Hu, M., and He, L.-Y.: Highly
352 time-resolved carbonaceous aerosol characterization in Yangtze River Delta of China: Composition, mixing state and
353 secondary formation, *Atmos. Environ.*, 64, 200-207, 10.1016/j.atmosenv.2012.09.059, 2013.

354 Huang, X. F., He, L. Y., Hu, M., Canagaratna, M. R., Sun, Y., Zhang, Q., Zhu, T., Xue, L., Zeng, L. W., Liu, X. G., Zhang, Y.
355 H., Jayne, J. T., Ng, N. L., and Worsnop, D. R.: Highly time-resolved chemical characterization of atmospheric submicron
356 particles during 2008 Beijing Olympic Games using an Aerodyne High-Resolution Aerosol Mass Spectrometer, *Atmospheric
357 Chemistry and Physics*, 10, 8933-8945, 10.5194/acp-10-8933-2010, 2010.

358 Huang, X. F., He, L. Y., Hu, M., Canagaratna, M. R., Kroll, J. H., Ng, N. L., Zhang, Y. H., Lin, Y., Xue, L., Sun, T. L., Liu, X.
359 G., Shao, M., Jayne, J. T., and Worsnop, D. R.: Characterization of submicron aerosols at a rural site in Pearl River Delta of
360 China using an Aerodyne High-Resolution Aerosol Mass Spectrometer, *Atmospheric Chemistry and Physics*, 11, 1865-1877,
361 10.5194/acp-11-1865-2011, 2011.

362 Huang, X. F., He, L. Y., Xue, L., Sun, T. L., Zeng, L. W., Gong, Z. H., Hu, M., and Zhu, T.: Highly time-resolved chemical

363 characterization of atmospheric fine particles during 2010 Shanghai World Expo, *Atmospheric Chemistry and Physics*, 12,
364 4897-4907, 10.5194/acp-12-4897-2012, 2012.

365 IPCC: Climate change: the physical science basis, Cambridge University Press, Cambridge, England, 2013.

366 Jimenez, J. L., Canagaratna, M. R., Donahue, N. M., Prevot, A. S. H., Zhang, Q., Kroll, J. H., DeCarlo, P. F., Allan, J. D., Coe,
367 H., Ng, N. L., Aiken, A. C., Docherty, K. S., Ulbrich, I. M., Grieshop, A. P., Robinson, A. L., Duplissy, J., Smith, J. D., Wilson,
368 K. R., Lanz, V. A., Hueglin, C., Sun, Y. L., Tian, J., Laaksonen, A., Raatikainen, T., Rautiainen, J., Vaattovaara, P., Ehn, M.,
369 Kulmala, M., Tomlinson, J. M., Collins, D. R., Cubison, M. J., Dunlea, J., Huffman, J. A., Onasch, T. B., Alfarra, M. R.,
370 Williams, P. I., Bower, K., Kondo, Y., Schneider, J., Drewnick, F., Borrmann, S., Weimer, S., Demerjian, K., Salcedo, D.,
371 Cottrell, L., Griffin, R., Takami, A., Miyoshi, T., Hatakeyama, S., Shimono, A., Sun, J. Y., Zhang, Y. M., Dzepina, K., Kimmel,
372 J. R., Sueper, D., Jayne, J. T., Herndon, S. C., Trimborn, A. M., Williams, L. R., Wood, E. C., Middlebrook, A. M., Kolb, C.
373 E., Baltensperger, U., and Worsnop, D. R.: Evolution of Organic Aerosols in the Atmosphere, *Science*, 326, 1525-1529,
374 10.1126/science.1180353, 2009.

375 Jolleys, M. D., Coe, H., McFiggans, G., Taylor, J. W., O'Shea, S. J., Breton, M. L., Bauguitte, S. J.-B., Moller, S., Carlo, P. D.,
376 Aruffo, E., Palmer, P. I., Lee, J. D., Percival, C. J., and Gallagher, M. W.: Properties and evolution of biomass burning organic
377 aerosol from Canadian boreal forest fire, *Atmos. Chem. Phys.*, 15, 3077-3095, 10.5194/acp-15-3077-2015, 2015.

378 Lüthi, Z. L., Škerlak, B., Kim, S. W., Lauer, A., Mues, A., Rupakheti, M., and Kang, S.: Atmospheric brown clouds reach the
379 Tibetan Plateau by crossing the Himalayas, *Atmos. Chem. Phys.*, 15, 6007-6021, 10.5194/acp-15-6007-2015, 2015.

380 Lau, W. K. M., Kim, M.-K., Kim, K.-M., and Lee, W.-S.: Enhanced surface warming and accelerated snow melt in the
381 Himalayas and Tibetan Plateau induced by absorbing aerosols, *Environ. Res. Lett.*, 5, 025204, 10.1088/1748-9326/5/2/025204,
382 2010.

383 Li, Y. J., Lee, B. P., Su, L., Fung, J. C. H., and Chan, C. K.: Seasonal characteristics of fine particulate matter (PM) based on
384 high-resolution time-of-flight aerosol mass spectrometric HR-ToF-AMS) measurements at the HKUST Supersite in Hong
385 Kong, *Atmospheric Chemistry and Physics*, 15, 37-53, 10.5194/acp-15-37-2015, 2015.

386 Marinoni, A., Cristofanelli, P., Laj, P., Duchi, R., Calzolari, F., Decesari, S., Sellegri, K., Vuillermoz, E., Verza, G. P., Villani,
387 P., and Bonasoni, P.: Aerosol mass and black carbon concentrations, a two year record at NCO-P (5079 m, Southern Himalayas),
388 *Atmos. Chem. Phys.*, 10, 8551-8562, 10.5194/acp-10-8551-2010, 2010.

389 Middlebrook, A. M., Bahreini, R., Jimenez, J. L., and Canagaratna, M. R.: Evaluation of Composition-Dependent Collection
390 Efficiencies for the Aerodyne Aerosol Mass Spectrometer using Field Data, *Aerosol Sci. Technol.*, 46, 258-271,
391 10.1080/02786826.2011.620041, 2012.

392 Ming, J., Xiao, C., Sun, J., Kang, S., and Bonasoni, P.: Carbonaceous particles in the atmosphere and precipitation of the Nam
393 Co region, central Tibet, *J. Environ. Sci.*, 22, 1748-1756, 10.1016/s1001-0742(09)60315-6, 2010.

394 Minguillón, M. C., Ripoll, A., Pérez, N., Prévôt, A. S. H., Canonaco, F., Querol, X., and Alastuey, A.: Chemical
395 characterization of submicron regional background aerosols in the western Mediterranean using an Aerosol Chemical
396 Speciation Monitor, *Atmospheric Chemistry and Physics*, 15, 6379-6391, 10.5194/acp-15-6379-2015, 2015.

397 Ng, N. L., Canagaratna, M. R., Zhang, Q., Jimenez, J. L., Tian, J., Ulbrich, I. M., Kroll, J. H., Docherty, K. S., Chhabra, P. S.,

398 Bahreini, R., Murphy, S. M., Seinfeld, J. H., Hildebrandt, L., Donahue, N. M., DeCarlo, P. F., Lanz, V. A., Prévôt, A. S. H.,
399 Dinar, E., Rudich, Y., and Worsnop, D. R.: Organic aerosol components observed in Northern Hemispheric datasets from
400 Aerosol Mass Spectrometry, *Atmospheric Chemistry and Physics*, 10, 4625-4641, 10.5194/acp-10-4625-2010, 2010.

401 Paatero, P., and Tapper, U.: Positive matrix factorization: A non-negative factor model with optimal utilization of error
402 estimates of data values, *Environmetrics*, 5, 111-126, 10.1002/env.3170050203, 1994.

403 Qian, Y., Flanner, M. G., Leung, L. R., and Wang, W.: Sensitivity studies on the impacts of Tibetan Plateau snowpack pollution
404 on the Asian hydrological cycle and monsoon climate, *Atmos. Chem. Phys.*, 11, 1929-1948, 10.5194/acp-11-1929-2011, 2011.

405 Ripoll, A., Mingüillón, M. C., Pey, J., Jimenez, J. L., Day, D. A., Sosedova, Y., Canonaco, F., Prévôt, A. S. H., Querol, X., and
406 Alastuey, A.: Long-term real-time chemical characterization of submicron aerosols at Montsec (southern Pyrenees,
407 1570ma.s.l.), *Atmos. Chem. Phys.*, 15, 2935-2951, 10.5194/acp-15-2935-2015, 2015.

408 Sjogren, S., Gysel, M., E. Weingartner, Alfarra, M. R., Duplissy, J., Cozic, J., Crosier, J., Coe, H., and Baltensperger, U.:
409 Hygroscopicity of the submicrometer aerosol at the high-alpine site Jungfraujoch, 3580m a.s.l., Switzerland, *Atmos. Chem.*
410 *Phys.*, 8, 5715-5729, 10.5194/acp-8-5715-2008, 2008.

411 Streets, D. G., Yarber, K. F., Woo, J. H., and Carmichael, G. R.: Biomass burning in Asia: Annual and seasonal estimates and
412 atmospheric emissions, *Global Biogeochem. Cycles*, 17, 1759-1768, 10.1029/2003gb002040, 2003.

413 Sun, Y. L., Zhang, Q., Schwab, J. J., Demerjian, K. L., Chen, W. N., Bae, M. S., Hung, H. M., Hogrefe, O., Frank, B., Rattigan,
414 O. V., and Lin, Y. C.: Characterization of the sources and processes of organic and inorganic aerosols in New York city with a
415 high-resolution time-of-flight aerosol mass spectrometer, *Atmospheric Chemistry and Physics*, 11, 1581-1602, 10.5194/acp-
416 11-1581-2011, 2011.

417 Ulbrich, I. M., Canagaratna, M. R., Zhang, Q., Worsnop, D. R., and Jimenez, J. L.: Interpretation of organic components from
418 Positive Matrix Factorization of aerosol mass spectrometric data, *Atmospheric Chemistry and Physics*, 9, 2891-2918,
419 10.5194/acp-9-2891-2009, 2009.

420 von Schneidemesser, E., Monks, P. S., Allan, J. D., Bruhwiler, L., Forster, P., Fowler, D., Lauer, A., Morgan, W. T., Paasonen,
421 P., Righi, M., Sindelarova, K., and Sutton, M. A.: Chemistry and the Linkages between Air Quality and Climate Change, *Chem.*
422 *Rev.*, 115, 3856-3897, 10.1021/acs.chemrev.5b00089, 2015.

423 Wan, X., Kang, S., Wang, Y., Xin, J., Liu, B., Guo, Y., Wen, T., Zhang, G., and Cong, Z.: Size distribution of carbonaceous
424 aerosols at a high-altitude site on the central Tibetan Plateau (Nam Co Station, 4730ma.s.l.), *Atmos. Res.*, 153, 155-164,
425 10.1016/j.atmosres.2014.08.008, 2015.

426 Wang, B., and French, H. M.: Climate Controls and High-Altitude Permafrost, Qinghai-Xizang (Tibet) Plateau, China,
427 *Permafrost and Periglacial Processes*, 5, 87-100, 10.1002/ppp.3430050203, 1994.

428 Wang, B., Liu, Y., Shao, M., Lu, S., Wang, M., Yuan, B., Gong, Z., He, L., Zeng, L., Hu, M., and Zhang, Y.: The contributions
429 of biomass burning to primary and secondary organics: A case study in Pearl River Delta (PRD), China, *Sci. Total. Environ.*,
430 569-570, 548-556, 10.1016/j.scitotenv.2016.06.153, 2016.

431 Xia, X., Zong, X., Cong, Z., Chen, H., Kang, S., and Wang, P.: Baseline continental aerosol over the central Tibetan plateau
432 and a case study of aerosol transport from South Asia, *Atmos. Environ.*, 45, 7370-7378, 10.1016/j.atmosenv.2011.07.067, 2011.

433 Xu, J., Zhang, Q., Li, X., Ge, X., Xiao, C., Ren, J., and Qin, D.: Dissolved organic matter and inorganic ions in a central
434 Himalayan glacier--insights into chemical composition and atmospheric sources, *Environ. Sci. Technol.*, 47, 6181-6188,
435 10.1021/es4009882, 2013.

436 Xu, J., Wang, Z., Yu, G., Qin, X., Ren, J., and Qin, D.: Characteristics of water soluble ionic species in fine particles from a
437 high altitude site on the northern boundary of Tibetan Plateau: Mixture of mineral dust and anthropogenic aerosol, *Atmos.*
438 *Res.*, 143, 43-56, 10.1016/j.atmosres.2014.01.018, 2014a.

439 Xu, J., Zhang, Q., Chen, M., Ge, X., Ren, J., and Qin, D.: Chemical composition, sources, and processes of urban aerosols
440 during summertime in northwest China: insights from high-resolution aerosol mass spectrometry, *Atmospheric Chemistry and*
441 *Physics*, 14, 12593-12611, 10.5194/acp-14-12593-2014, 2014b.

442 Xu, J. Z., Zhang, Q., Wang, Z. B., Yu, G. M., Ge, X. L., and Qin, X.: Chemical composition and size distribution of summertime
443 PM_{2.5} at a high altitude remote location in the northeast of the Qinghai–Xizang (Tibet) Plateau: insights into aerosol sources
444 and processing in free troposphere, *Atmospheric Chemistry and Physics*, 15, 5069-5081, 10.5194/acp-15-5069-2015, 2015.

445 You, C., Xu, C., Xu, B., Zhao, H., and Song, L.: Levoglucosan evidence for biomass burning records over Tibetan glaciers,
446 *Environ. Pollu.*, 216, 173-181, 10.1016/j.envpol.2016.05.074, 2016.

447 Zhang, Q., Jimenez, J. L., Canagaratna, M. R., Ulbrich, I. M., Ng, N. L., Worsnop, D. R., and Sun, Y.: Understanding
448 atmospheric organic aerosols via factor analysis of aerosol mass spectrometry: a review, *Anal Bioanal Chem*, 401, 3045-3067,
449 10.1007/s00216-011-5355-y, 2011.

450 Zhang, Y., Tang, L., Wang, Z., Yu, H. X., Sun, Y. L., Liu, D., Qin, W., Canonaco, F., Prévôt, A. S. H., Zhang, H. L., and Zhou,
451 H. C.: Insights into characteristics, sources, and evolution of submicron aerosols during harvest seasons in the Yangtze River
452 delta region, China, *Atmospheric Chemistry and Physics*, 15, 1331-1349, 10.5194/acp-15-1331-2015, 2015.

453 Zhao, Z., Cao, J., Shen, Z., Xu, B., Zhu, C., Chen, L. W. A., Su, X., Liu, S., Han, Y., Wang, G., and Ho, K.: Aerosol particles
454 at a high-altitude site on the Southeast Tibetan Plateau, China: Implications for pollution transport from South Asia, *J. Geophys.*
455 *Res. Atmos.*, 118, 11,360-311,375, 10.1002/jgrd.50599, 2013.

456

457

458

459

460

461

462

463

464

Table1. Comparison between mass spectra of different OA with reference spectra.

Reference spectra		Pearson Correlation Coefficient (N=100)			Citation
		BBOA	OOA-BB	OOA	
Ambient measurement	900m above fire	0.91	0.56	0.34	Brito et al. (2014)
	3h downwind	0.51	0.97	0.91	Brito et al. (2014)
	MO-OOA	0.69	0.86	0.69	Hu et al. (2016)
	BBOA	0.85	0.38	0.11	Hu et al. (2016)
Laboratory simulation	wood of pin	0.91	0.61	0.42	He et al. (2010)
	rice straw	0.94	0.6	0.36	He et al. (2010)

465

466

467

468

469

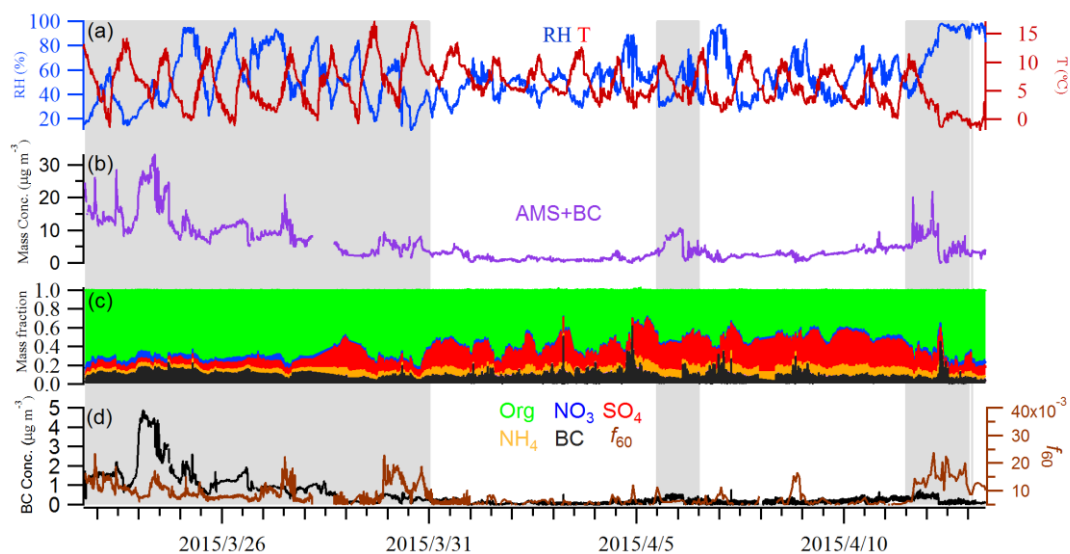
470

471

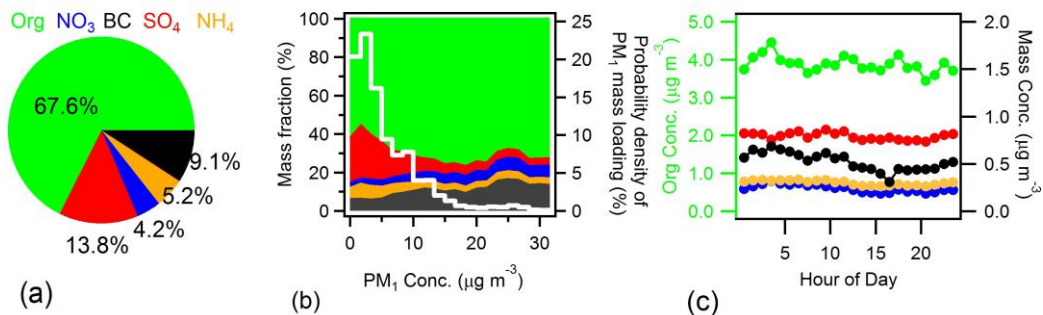
472



473
474 **Fig.1** The location of the sampling site at Mt. Yulong (27.2°N 100.2°E, 3410 m a.s.l.).



475
476 **Fig.2** Time series of (a) relative humidity and temperature; (b) total mass concentrations from AMS plus black carbon (c) mass
477 fractions of different chemical species; (d) concentrations of black carbon and f_{60} . The gray background denotes three biomass
478 burning events (identified in Section 4.1).



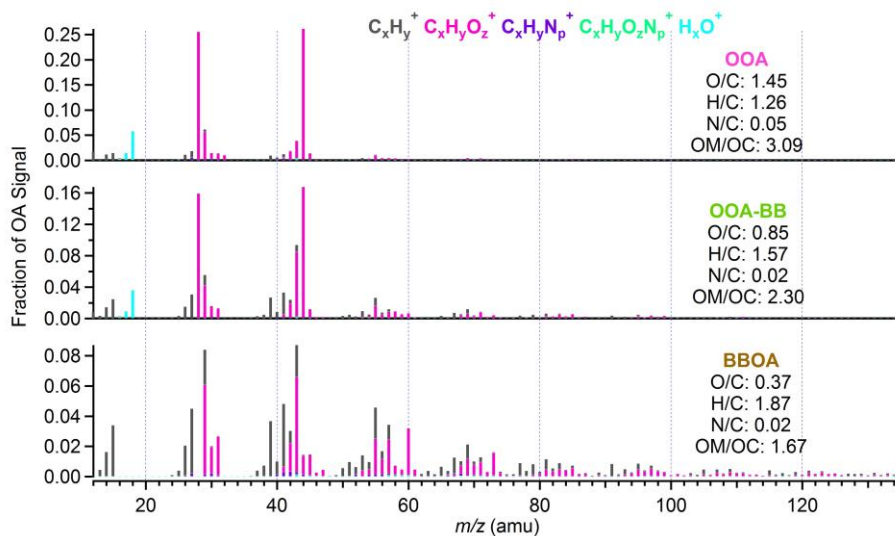
479

480

481

482

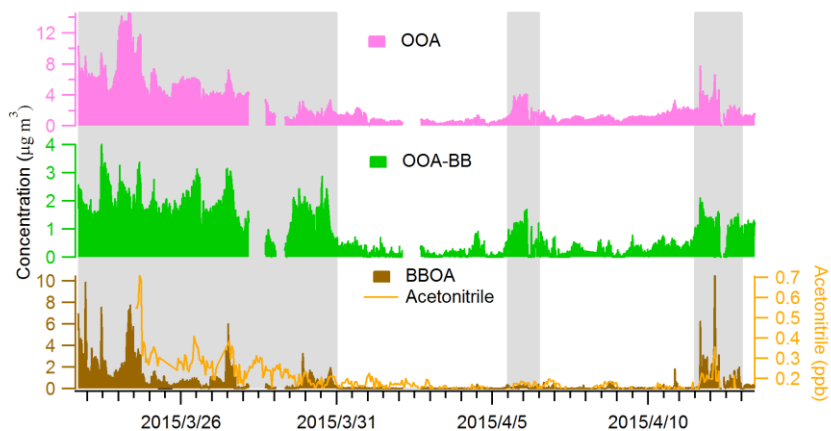
Fig.3 (a) average chemical composition of the whole campaign; (b) the mass fractions of PM₁ species as a function of PM₁ mass loading (left axis), with the white line representing the probability density of PM₁ mass loadings (right axis); (c) the diel cycle of different species, with the left axis for organics, and the right axis for the rest components.



483

484

Fig.4 The mass spectra of each factor resolved by PMF, together with atomic ratios of each factor.



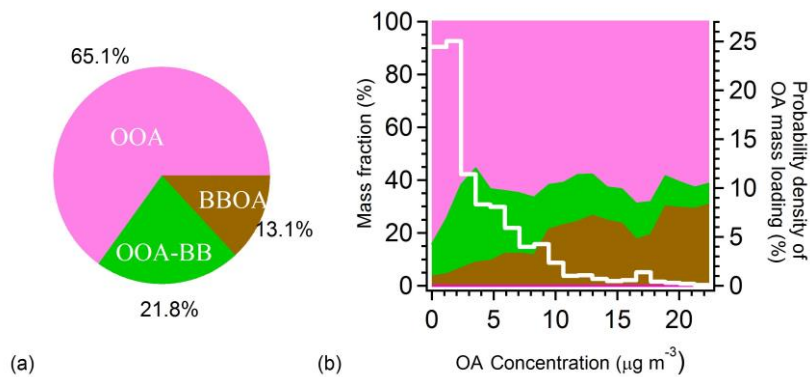
485

486

Fig.5 The time series of three OA factors resolved by PMF, together with acetonitrile, a gas phase tracer for biomass burning.

487

The grey background areas denote the biomass burning events (identified in Section 4.1).



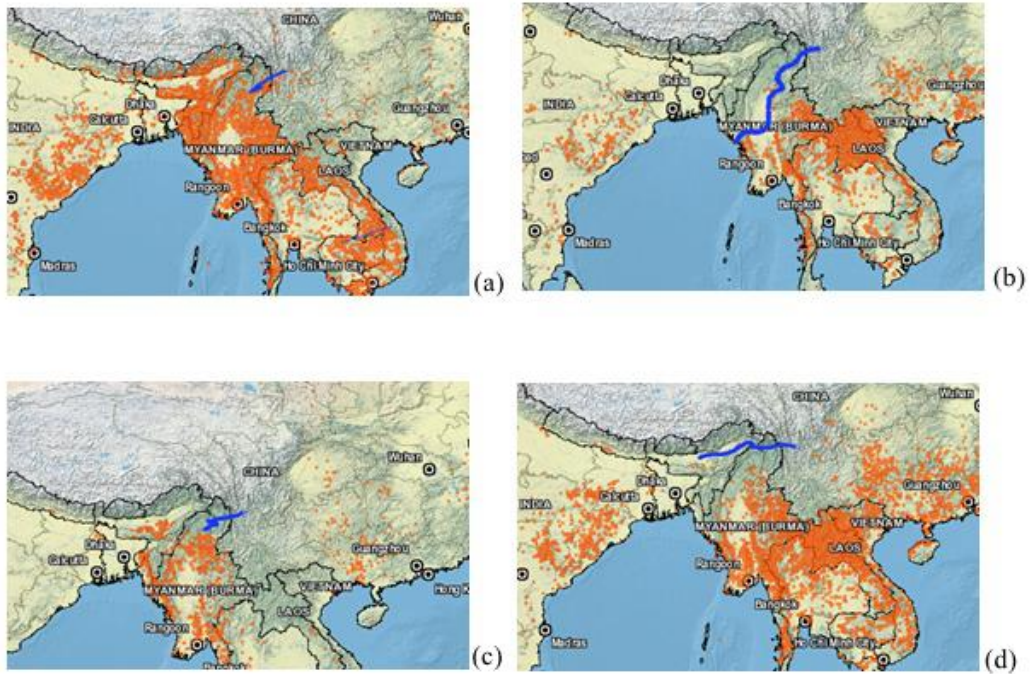
488

489

Fig.6 (a) contribution of each factor to the total OA mass; (b) fractions of OA factor (left axis) and probability density of OA

490

concentration (white line, right axis) as a function of OA mass loading.



491

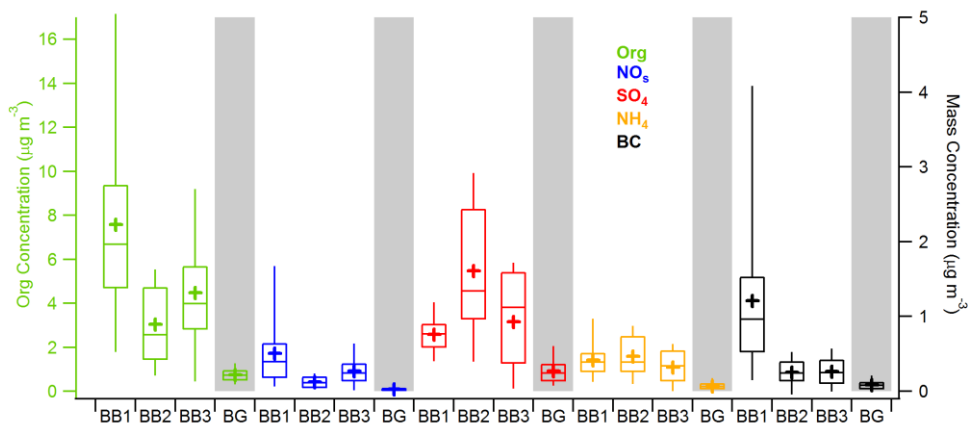
492 **Fig.7 Occurrence of wildfire derived from MODIS images and back trajectories (blue lines) from WRF model (a) first biomass**

493 **burning event: March 22nd – 30th; (b) second biomass burning event: April 5th – 6th; (c) third biomass burning event: April 11th**

494

– 12th; (d) background: April 1st – 4th.

495



496

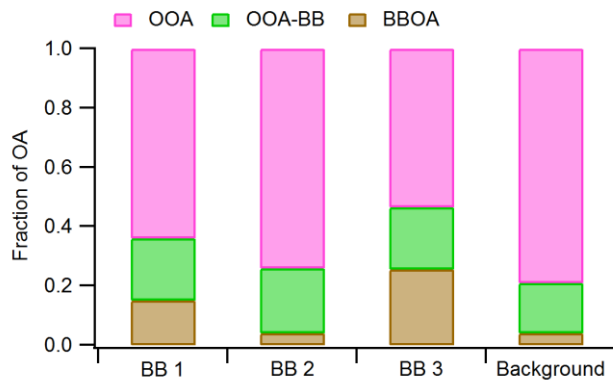
497 **Fig.8 Comparison of chemical compositions between three biomass burning events (BB1, BB2, BB3) and background conditions**

498 (BG, highlighted by light gray color). Boxes denote median, 25th and 75th percentiles; whiskers represent 5th and 95th percentiles;

499 crosses represent mean values. Organic aerosols are represented by the left axis while other species are represented by the right

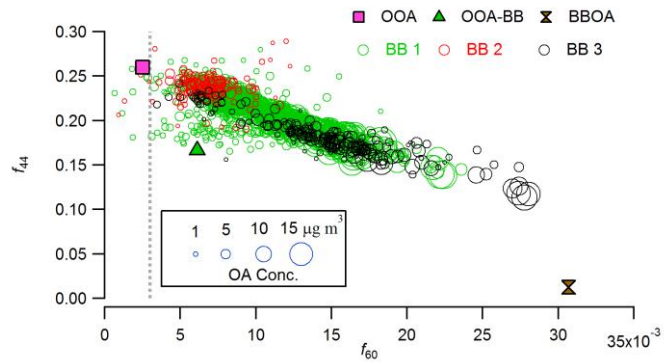
500 axis.

501



502

503 **Fig.9 The relative contribution of different types of OA during three biomass burning events and background condition.**



504

505

Fig.10 f_{44} as a function of f_{60} (f_{44} vs. f_{60} triangle plot) of the three biomass burning events, sized by OA concentration.